

1 **Antiviral treatment of SARS-CoV-2-infected hamsters reveals a weak effect of favipiravir**
2 **and a complete lack of effect for hydroxychloroquine**

3 Suzanne JF Kaptein*¹, Sofie Jacobs^{#1}, Lana Langendries^{#1}, Laura Seldeslachts^{#2}, Sebastiaan
4 ter Horst¹, Laurens Liesenborghs¹, Bart Hens³, Valentijn Vergote¹, Elisabeth Heylen¹, Elke
5 Maas¹, Carolien De Keyzer¹, Lindsey Bervoets¹, Jasper Rymenants¹, Tina Van Buyten¹,
6 Hendrik Jan Thibaut¹, Kai Dallmeier¹, Robbert Boudewijns¹, Jens Wouters⁴, Patrick
7 Augustijns³, Nick Verougstraete⁵, Christopher Cawthorne⁶, Birgit Weynand⁷, Pieter Annaert³,
8 Isabel Spriet⁸, Greetje Vande Velde², Johan Neyts^{*1}, Joana Rocha-Pereira^{#1}, Leen Delang^{*#1}

9 ¹KU Leuven Department of Microbiology, Immunology and Transplantation, Rega Institute for
10 Medical Research, Laboratory of Virology and Chemotherapy, B-3000 Leuven, Belgium

11 ²KU Leuven Department of Imaging and Pathology, Biomedical MRI and MoSAIC, B-3000
12 Leuven, Belgium

13 ³KU Leuven, Department of Pharmaceutical and Pharmacological Sciences, Drug Delivery &
14 Disposition, Box 921, 3000 Leuven, Belgium

15 ⁴KU Leuven Department of Imaging and Pathology, Molecular Small Animal Imaging Centre
16 (MoSAIC), B-3000 Leuven, Belgium

17 ⁵Department of Laboratory Medicine, Ghent University Hospital, Ghent, Belgium

18 ⁶KU Leuven, Department of Imaging and Pathology, Nuclear Medicine and Molecular Imaging,
19 B-3000 Leuven, Belgium

20 ⁷KU Leuven Department of Imaging and Pathology, Translational Cell and Tissue Research,
21 B-3000 Leuven, Belgium; Division of Translational Cell and Tissue Research

22 ⁸Pharmacy Dpt, University Hospitals Leuven and Department of Pharmaceutical and
23 Pharmacological Sciences, KU Leuven – University of Leuven, Belgium

24 *corresponding authors: suzanne.kaptein@kuleuven.be, johan.neyts@kuleuven.be,
25 joana.rochapereira@kuleuven.be, leen.delang@kuleuven.be

26 # equal contribution

27 **Abstract**

28 SARS-CoV-2 rapidly spread around the globe after its emergence in Wuhan in December
29 2019. With no specific therapeutic and prophylactic options available, the virus was able to
30 infect millions of people. To date, close to half a million patients succumbed to the viral disease,
31 COVID-19. The high need for treatment options, together with the lack of small animal models
32 of infection has led to clinical trials with repurposed drugs before any preclinical *in vivo*
33 evidence attesting their efficacy was available. We used Syrian hamsters to establish a model
34 to evaluate antiviral activity of small molecules in both an infection and a transmission setting.
35 Upon intranasal infection, the animals developed high titers of SARS-CoV-2 in the lungs and
36 pathology similar to that observed in mild COVID-19 patients. Treatment of SARS-CoV-2-
37 infected hamsters with favipiravir or hydroxychloroquine (with and without azithromycin)
38 resulted in respectively a mild or no reduction in viral RNA and infectious virus. Micro-CT scan
39 analysis of the lungs showed no improvement compared to non-treated animals, which was
40 confirmed by histopathology. In addition, both compounds did not prevent virus transmission
41 through direct contact and thus failed as prophylactic treatments. By modelling the PK profile
42 of hydroxychloroquine based on the trough plasma concentrations, we show that the total lung
43 exposure to the drug was not the limiting factor. In conclusion, we here characterized a hamster
44 infection and transmission model to be a robust model for studying *in vivo* efficacy of antiviral
45 compounds. The information acquired using hydroxychloroquine and favipiravir in this model
46 is of critical value to those designing (current and) future clinical trials. At this point, the data
47 here presented on hydroxychloroquine either alone or combined with azithromycin (together
48 with previously reported *in vivo* data in macaques and ferrets) provide no scientific basis for
49 further use of the drug in humans.

50 **Introduction**

51 The severe acute respiratory syndrome coronavirus 2 (SARS-CoV-2) first emerged in Wuhan,
52 China in December 2019¹. From there, the virus rapidly spread around the globe, infecting
53 more than 8 million people so far (June 18) [<https://covid19.who.int/>]. SARS-CoV-2 is the
54 causative agent of coronavirus disease 2019 (COVID-19). Common clinical manifestations of
55 COVID-19 are fever, dry cough, paired in a minority of patients with difficult breathing, muscle
56 and/or joint pain, headache/dizziness, decreased sense of taste and smell, diarrhea, and
57 nausea². A small subset of patients will develop to acute respiratory distress syndrome
58 (ARDS), characterized by difficult breathing and low blood oxygen levels, which may directly
59 result into respiratory failure². In addition, an overreaction of the host's immune and
60 inflammatory responses can result in a vast release of cytokines ('cytokine storm'), inducing
61 sepsis and multi-organ damage, which may lead to organ failure³. To date, more than 440,000
62 patients worldwide succumbed to COVID-19. Hence, in response to the ongoing pandemic
63 there is a desperate need for therapeutic and prophylactic options.

64 At present, no specific antiviral drugs have been developed and approved to treat infections
65 with human coronaviruses. Nonetheless, antiviral drugs could fulfill an important role in the
66 treatment of COVID-19 patients. Slowing down the replication of SARS-CoV-2 by antiviral
67 treatment could be beneficial and prevent or alleviate symptoms. In addition, antiviral drugs
68 could be used as prophylaxis to protect health care workers and high-risk groups. However, a
69 specific, highly potent antiviral drug for SARS-CoV-2 will take years to develop and evaluate
70 in clinical studies. Therefore, the main focus for COVID-19 treatment on the short term is on
71 the repurposing of drugs that have been approved for other diseases⁴. Repurposed drugs can
72 however not be expected to be highly potent inhibitors of SARS-CoV-2, since these were not
73 developed and optimized specifically against this virus. In cell culture, several repurposed
74 drugs inhibit SARS-CoV-2 replication^{5,6}. Although preclinical *in vivo* evidence evaluating the
75 efficacy of some of these repurposed drugs for COVID-19 treatment is lacking, clinical trials

76 have already been conducted or are currently ongoing. Two such drugs are
77 hydroxychloroquine and favipiravir.

78 Hydroxychloroquine (HCQ) is an anti-malaria drug that has been widely used to treat patients
79 with malaria, rheumatoid arthritis and systemic lupus erythematosus. This drug is also able to
80 inhibit a broad range of viruses from different virus families in cell culture, including
81 coronaviruses (SARS-CoV-1, MERS-CoV)^{7,8}. Favipiravir is a broad-spectrum antiviral drug that
82 has been approved in Japan since 2014 to treat pandemic influenza virus infections⁹. Both
83 drugs have shown antiviral efficacy against SARS-CoV-2 in Vero E6 cells¹⁰, albeit modest for
84 favipiravir¹⁰⁻¹². Enzymatic assays with the SARS-CoV-2 RNA-dependent RNA polymerase
85 demonstrated that favipiravir acts as a nucleotide analog via a combination of chain
86 termination, slowed viral RNA synthesis and lethal mutagenesis¹². However, proof of *in vivo*
87 efficacy in animal models is still lacking for both drugs. Nevertheless, clinical trials were
88 initiated early on in the pandemic to assess the efficacy of HCQ and favipiravir to treat COVID-
89 19 patients. For HCQ, these trials were small anecdotal studies or inconclusive small
90 randomized trials¹³ and thus did not lead to conclusive results. Despite the lack of clear
91 evidence, HCQ is currently being widely used for the treatment of COVID-19, often in
92 combination with a second-generation macrolide such as azithromycin. Results from animal
93 models and rigorous randomized controlled trials are thus required to clarify the efficacy of
94 HCQ and favipiravir in the treatment of COVID-19 patients.

95 Infection models in small animals are crucial for the evaluation and development of antiviral
96 drugs. Although rhesus and cynomolgus macaques seem to be relevant models for studying
97 the early stages of COVID-19 infection in humans¹⁴, preclinical models using smaller animals
98 are essential to ensure efficient and ethical allocation of resources towards designing
99 (relevant) preclinical and clinical efficacy studies. Syrian hamsters are permissive to SARS-
100 CoV-2 and develop mild lung disease similar to the disease observed in early-stage COVID-
101 19 patients^{15,16}. Nevertheless, evidence of antiviral efficacy of repurposed drugs in small animal
102 models is lacking to date. In this work, we characterized Syrian hamsters as a model for the

103 evaluation of antiviral drugs in therapeutic and prophylactic settings against SARS-CoV-2. We
104 then used this model to evaluate the antiviral efficacy of HCQ and favipiravir against SARS-
105 CoV-2 in infected hamsters and in a transmission setting.

106 **Material and Methods**

107 *SARS-CoV-2*

108 The SARS-CoV-2 strain used in this study, BetaCov/Belgium/GHB-03021/2020 (EPI ISL
109 407976|2020-02-03), was recovered from a nasopharyngeal swab taken from a RT-qPCR-
110 confirmed asymptomatic patient who returned from Wuhan, China in the beginning of February
111 2020¹⁷. A close relation with the prototypic Wuhan-Hu-1 2019-nCoV (GenBank accession
112 number MN908947.3) strain was confirmed by phylogenetic analysis. Infectious virus was
113 isolated by serial passaging on HuH7 and Vero E6 cells¹⁶; passage 6 virus was used for the
114 studies described here. The titer of the virus stock was determined by end-point dilution on
115 Vero E6 cells by the Reed and Muench method. Live virus-related work was conducted in the
116 high-containment A3 and BSL3⁺ facilities of the KU Leuven Rega Institute (3CAPS) under
117 licenses AMV 30112018 SBB 219 2018 0892 and AMV 23102017 SBB 219 20170589
118 according to institutional guidelines.

119 *Cells*

120 Vero E6 cells (African green monkey kidney, ATCC CRL-1586) were cultured in minimal
121 essential medium (Gibco) supplemented with 10% fetal bovine serum (Integro), 1% L-
122 glutamine (Gibco) and 1% bicarbonate (Gibco). End-point titrations were performed with
123 medium containing 2% fetal bovine serum instead of 10%.

124 *Compounds*

125 Favipiravir was purchased from BOC Sciences (USA). Hydroxychloroquine sulphate was
126 acquired from Acros Organics. For *in vivo* treatment, a 30 mg/mL favipiravir suspension was
127 prepared in 0.4% carboxymethylcellulose and a 20 mg/mL hydroxychloroquine sulphate
128 solution in 10% DMSO, 18% Cremophor, and 72% water. Azithromycin was provided by the
129 hospital pharmacy of the University Hospitals Leuven (Belgium) as a 40 mg/ml oral solution
130 (Zitromax[®]) which was diluted to 5 mg/mL with an aqueous medium consisting of 0.6% xanthan
131 gum as viscosity enhancer.

132 *SARS-CoV-2 infection model in hamsters*

133 The hamster infection model of SARS-CoV-2 has been described before¹⁶. In brief, wild-type
134 Syrian hamsters (*Mesocricetus auratus*) were purchased from Janvier Laboratories and were
135 housed per two in ventilated isolator cages (IsoCage N Biocontainment System, Tecniplast)
136 with *ad libitum* access to food and water and cage enrichment (wood block). Housing
137 conditions and experimental procedures were approved by the ethical committee of animal
138 experimentation of KU Leuven (license P065-2020).

139 Female hamsters of 6-10 weeks old were anesthetized with ketamine/xylazine/atropine and
140 inoculated intranasally with 50 µL containing 2×10^6 TCID₅₀. Drug treatment was initiated 1h
141 before infection. Favipiravir was administered twice daily by oral gavage, starting with a loading
142 dose of 600 mg/kg/day on the first day. On consecutive days, 300 mg/kg/day favipiravir was
143 administered until the day of sacrifice. Hydroxychloroquine sulphate (50 mg/kg) was
144 administered once daily by intraperitoneal (ip) injection for 4 days. Azithromycin (10 mg/kg)
145 was administered once daily by oral gavage using a 5 mg/ml dilution of Zitromax®. Hamsters
146 were daily monitored for appearance, behavior and weight. At day 4 post infection (pi),
147 hamsters were euthanized by ip injection of 500 µL Dolethal (200mg/mL sodium pentobarbital,
148 Vétoquinol SA). Tissues [lungs, small intestine (ileum)] and stool were collected, and viral RNA
149 and infectious virus were quantified by RT-qPCR and end-point virus titration, respectively.
150 Blood samples were collected at day 4 pi for PK analysis of HCQ.

151 *SARS-CoV-2 transmission model in hamsters*

152 The hamster transmission model of SARS-CoV-2 via direct contact has been described
153 previously^{15,18}. Briefly, index hamsters (6-10 weeks old) were infected as described above. At
154 the day of exposure, sentinel hamsters were co-housed with index hamsters that had been
155 intranasally inoculated with SARS-CoV-2 one day earlier. Index and sentinel hamsters were
156 sacrificed at day 4 pi (post-exposure in the case of the sentinels) and the viral load in lung,
157 ileum and stool was determined, as described above. For prophylactic testing of drugs, sentinel

158 hamsters were treated daily for 5 consecutive days with either hydroxychloroquine or
159 favipiravir, starting 1 day prior to exposure to the index hamster.

160 To study the contribution of the fecal-oral route to the overall transmission of SARS-CoV-2,
161 index hamsters were inoculated as described earlier. On day 1 or 3 pi, the index hamsters
162 were sacrificed after which sentinel hamsters were placed in the dirty cages of the index
163 hamsters. Food grids and water bottles were replaced by clean ones to minimize virus
164 transmission via food or water. At day 4 post exposure, the sentinels were sacrificed. Tissues
165 (lung, ileum and stool) were collected from index and sentinel hamsters and processed for
166 detection of viral RNA and infectious virus.

167 *PK analysis of hydroxychloroquine and metabolite in plasma*

168 Hydroxychloroquine (HCQ) and its active metabolite desethylhydroxychloroquine (DHCQ)
169 were quantified in EDTA-plasma samples. A total of (i) 50 µL sample and (ii) 10 µL of internal
170 standard (IS) solution (hydroxychloroquine-d4 1500 ng/mL in water) were added to a tube and
171 mixed. After addition of 50 µL 5% perchloric acid, samples were shaken for 5 min and
172 centrifuged for 5 min at 16,162 g. Five µL of the supernatant was injected onto the HPLC-
173 column.

174 HPLC analysis was performed using a Shimadzu Prominence system (Shimadzu, Kioto,
175 Japan) equipped with a Kinetex C18 column (100mm length x 2.1mm i.d., 2.6 µm particle size)
176 (Phenomenex, Torrance, CA, USA) at 50°C. A 6 min gradient of mobile phase A (0.1% formic
177 acid (FA) in water) and B (0.1% FA in acetonitrile) with a flow rate of 0.4 mL/min was used for
178 elution of the compounds. The mass spectrometer (MS) was a Triple Quad 5500 (Sciex,
179 Framingham, MA, USA) with an electrospray ionization source (ESI) in positive ion mode,
180 using multiple reaction monitoring (MRM). The monitored transitions were 336.8 to 248.0 m/z,
181 307.8 to 130.0 m/z and 340.8 to 252.0 m/z for HCQ, DHCQ, and HCQ-d4, respectively. The
182 used collision energy for all the transitions was 30 V. Calibration curves for both HCQ (linear
183 1/x weighting) and DHCQ (quadratic 1/x² weighting) were between 10 and 2250 ng/mL.

184 Between-run imprecision over all QC levels (10, 25, 400, 2000 ng/mL) ranged from 2.84 to
185 11.4% for HCQ and from 5.19 to 10.2% for DHCQ.

186 *Calculation of hydroxychloroquine concentration in the lung cytosol*

187 Starting from the measured total trough plasma concentrations measured at sacrifice after 4
188 or 5 days of HCQ treatment, total lung cytosolic concentrations of HCQ were calculated. First,
189 the mean trough total plasma concentration of HCQ was used as a starting point to estimate
190 the whole blood concentrations considering a blood to plasma ratio of 7.2, as reported by Tett
191 and co-workers¹⁹ and as mentioned in the SmPC of Plaquenil® (Sanofi, Paris, France)
192 (**Equation 1**).

193
$$\text{whole blood concentration} = \text{plasma concentration} \times 7.2$$

194 (**Equation 1**)

195 Relying on the experimental K_p (tissue versus whole blood partition coefficient) values in rats,
196 the total lung tissue concentrations of HCQ was determined. Based on the partition values as
197 reported by Wei et al.²⁰, a lung K_p value of 50 was applied to estimate the total lung
198 concentration (**Equation 2**).

199
$$\text{Total lung tissue concentration} = \text{mean blood concentration} \times 50$$

200 (**Equation 2**)

201 Subsequently, as the HCQ efficacy target is intracellular, the cytosolic / total HCQ
202 concentration ratio was estimated, based on (i) relative lysosomal lung tissue volume, as well
203 as the contributions of interstitial and intracellular volumes to total lung volume and (ii) the pH
204 partition theory applying a pKa value of HCQ of 9.67. Based on these calculations (data not
205 shown), lung cytosolic HCQ concentrations are corresponding to 6% of the total lung tissue
206 concentration (**Equation 3**).

207
$$\text{Total cytosolic lung tissue concentration} = \text{total lung tissue concentration} \times 0.06$$

208 (**Equation 3**)

209 The calculated total cytosolic lung concentration was compared with EC₅₀ concentrations
210 previously reported in literature, ranging from 0.72 μ M to 17.3 μ M²¹⁻²³.

211 *SARS-CoV-2 RT-qPCR*

212 Hamster tissues were collected after sacrifice and were homogenized using bead disruption
213 (Precellys) in 350 μ L RLT buffer (RNeasy Mini kit, Qiagen) and centrifuged (10,000 rpm, 5 min)
214 to pellet the cell debris. RNA was extracted according to the manufacturer's instructions. To
215 extract RNA from serum, the NucleoSpin kit (Macherey-Nagel) was used. Of 50 μ L eluate, 4
216 μ L was used as a template in RT-qPCR reactions. RT-qPCR was performed on a
217 LightCycler96 platform (Roche) using the iTaq Universal Probes One-Step RT-qPCR kit
218 (BioRad) with N2 primers and probes targeting the nucleocapsid¹⁶. Standards of SARS-CoV-
219 2 cDNA (IDT) were used to express viral genome copies per mg tissue or per mL serum.

220 *End-point virus titrations*

221 Lung tissues were homogenized using bead disruption (Precellys) in 350 μ L minimal essential
222 medium and centrifuged (10,000 rpm, 5min, 4°C) to pellet the cell debris. To quantify infectious
223 SARS-CoV-2 particles, endpoint titrations were performed on confluent Vero E6 cells in 96-
224 well plates. Viral titers were calculated by the Reed and Muench method using the Lindenbach
225 calculator²⁴ and were expressed as 50% tissue culture infectious dose (TCID₅₀) per mg tissue.

226 *Histology*

227 For histological examination, the lungs were fixed overnight in 4% formaldehyde and
228 embedded in paraffin. Tissue sections (5 μ m) were analyzed after staining with hematoxylin
229 and eosin and scored blindly for lung damage by an expert pathologist. The scored
230 parameters, to which a cumulative score of 1 to 3 was attributed, were the following:
231 congestion, intral-alveolar hemorrhagic, apoptotic bodies in bronchus wall, necrotizing
232 bronchiolitis, perivascular edema, bronchopneumonia, perivascular inflammation,
233 peribronchial inflammation and vasculitis.

234 *Micro-computed tomography (CT) and image analysis*

235 Micro-CT data of hamster lungs were acquired *in vivo* using dedicated small animal micro-CT
236 scanners, either using the X-cube (Molecubes, Ghent, Belgium) or the Skyscan 1278 (Bruker
237 Belgium, Kontich, Belgium). In brief, hamsters were anaesthetized using isoflurane (2-3% in
238 oxygen) and installed in prone position into the X-cube scanner using a dedicated imaging
239 bed. A scout view was acquired and the lung was selected for a non-gated, helical CT
240 acquisition using the High-Resolution CT protocol, with the following parameters: 50 kVp, 960
241 exposures, 32 ms/projection, 350 μ A tube current, rotation time 120 s. Data were reconstructed
242 with 100 μ m isotropic voxel size using a regularized statistical (iterative) image reconstruction
243 algorithm²⁵. On the SkyScan1278, hamsters were scanned in supine position under isoflurane
244 anesthesia and the following scan parameters were used: 55 kVp X-ray source voltage and
245 500 μ A current combined with a composite X-ray filter of 1 mm aluminium, 80 ms exposure
246 time per projection, acquiring 4 projections per step with 0.7° increments over a total angle of
247 220°, and 10 cm field of view covering the whole body producing expiratory weighted 3D data
248 sets with 50 μ m isotropic reconstructed voxel size²⁶. Each scan took approximately 3 minutes.

249 Visualization and quantification of reconstructed micro-CT data were performed with
250 DataViewer and CTan software (Bruker Belgium). As primary outcome measure, a semi-
251 quantitative scoring of micro-CT data was performed as previously described²⁵. Visual
252 observations were blindly scored (from 0 – 2 depending on severity, both for parenchymal and
253 airway disease) on 5 different, predefined transversal tomographic sections throughout the
254 entire lung image for both lung and airway disease by two independent observers and
255 averaged. Scores for the 5 sections were summed up to obtain a score from 0 to 10 reflecting
256 severity of lung and airway abnormalities compared to scans of healthy, WT control hamsters.
257 As secondary measures, imaging-derived biomarkers (non-aerated lung volume, aerated lung
258 volume, total lung volume and respective densities within these volumes) were quantified as
259 previously^{16,26,27} or a manually delineated volume of interest covering the lung, avoiding the

260 heart and main blood vessels. The threshold used to distinguish aerated from non-aerated
261 lung volume was manually defined and kept constant for all data sets^{26,27}.

262 *Statistics*

263 GraphPad Prism (GraphPad Software, Inc.). was used to perform statistical analysis.
264 Statistical significance was determined using the non-parametric Mann Whitney U-test. P
265 values of ≤ 0.05 were considered significant.

266 **Results**

267 *Characterization of hamster model for antiviral drug evaluation*

268 We further characterized SARS-CoV-2 infection and readouts of disease in hamsters to be
269 able to use this model for the evaluation and development of antiviral drugs. To investigate
270 SARS-CoV-2 replication and shedding, the lung, ileum and stool of infected hamsters were
271 harvested at different time points post-infection (pi) for viral RNA quantification by RT-qPCR.
272 Infectious virus titers were additionally determined in lung samples. SARS-CoV-2 efficiently
273 replicates in the lungs of the hamsters, with viral RNA being detected in the lungs from day 1
274 pi and reaching a maximum level of ~ 7 \log_{10} RNA copies/mg tissue at 4 days pi (Fig 1A). A
275 similar kinetic profile was found in the ileum and stool samples, albeit at lower levels of 2-3
276 \log_{10} RNA copies/mg of tissue. Titrations of homogenized lung tissue contained infectious
277 particles from 1 day pi and reached levels of ~ 5 \log_{10} TCID₅₀/mg tissue from day 2 pi onwards
278 (Fig 1B), which is in line with the viral RNA levels. Infected animals displayed a slight weight
279 loss of about 5% by day 2 pi, which was completely resolved by day 4 pi (Fig 1C). No other
280 signs of disease or distress were observed in the hamsters at any time point pi.

281 Alike to what is currently done in clinical practice, we evaluated the development of lung
282 disease in a non-invasive way by micro-computed tomography (micro-CT) scanning the
283 infected animals under isoflurane gas anesthesia²⁸. Dense lung infiltrations and bronchial
284 dilation were simultaneously present from day 3 pi onwards, becoming more pronounced at
285 day 4 pi. Longitudinal follow-up of radiological pathology showed signs of multifocal pulmonary
286 infiltrates and lung consolidation on day 3 pi (Fig 1D). Analysis by H&E staining of lungs of
287 infected hamsters at day 4 pi showed signs of bronchopneumonia and peribronchial
288 inflammation, which were not present at the day of inoculation (Fig 1E).

289 *Evaluation of in vivo efficacy of hydroxychloroquine and favipiravir*

290 Next, we treated hamsters with antiviral molecules for four consecutive days starting one hour
291 before intranasal infection with SARS-CoV-2. At day 4 pi, a micro-CT scan was performed,

292 after which the animals were sacrificed and organs were collected for quantification of viral
293 RNA, infectious virus titers and lung histopathology (Fig 2A). Twice-daily treatment with
294 favipiravir was done orally with a loading dose of 600 mg/kg/day at day 0 pi and 300 mg/kg/day
295 from day 1 pi onwards. Favipiravir-treated hamsters presented a decrease of 0.9 \log_{10} RNA
296 copies/mg lung tissue, compared to untreated infected hamsters (Fig 2B); a lesser effect was
297 observed in the ileum and stool of treated animals (Fig 2B). A modest reduction in infectious
298 titers of 0.5 \log_{10} TCID₅₀/mg was observed in the lungs of favipiravir-treated animals (Fig. 2C).
299 Treatment with favipiravir caused over 5% weight loss at day 3 and 4 pi, which is slightly more
300 than that of the untreated animals (Fig. 2D). This could be due to the effect of administering a
301 relatively high volume of compound per os (which was at the limit of 10 mL/kg/ day) or due to
302 some toxicity of the molecule. Despite the very modest reduction in viral load, no obvious
303 change (improvement or worsening) of the rather subtle radiological and histological lung
304 pathology could be observed in favipiravir-treated hamsters (Fig. 2E-G). Quantification of
305 micro-CT-derived biomarkers support these observations and quantify a relatively small
306 burden of radiological lung consolidation upon infection that does not change with favipiravir
307 treatment (Fig. 2F).

308 HCQ sulphate was tested alone or in combination with azithromycin at a dose of 50 mg/kg/day
309 (equivalent to 39 mg/kg HCQ base) administered intraperitoneally once daily. When in
310 combination, azithromycin was given orally once daily at a dose of 10 mg/kg/day. Treatment
311 with HCQ alone resulted in a very modest reduction of 0.3 \log_{10} viral RNA copies/mg lung, and
312 no reduction in viral RNA load in the ileum or stool compared to untreated infected hamsters
313 (Fig 2B). When combined with azithromycin, no additional reduction of viral RNA was observed
314 in the organs of infected animals (Fig 2B). Virus titrations of the lungs also revealed no
315 significant reduction after treatment with HCQ alone or in combination with azithromycin (Fig
316 2C). The weight loss of the animals treated with HCQ follows along the lines of the untreated
317 animals with < 5% weight loss during the whole experiment, while the combination treatment
318 with azithromycin caused a slightly greater weight loss at day 1 and 2 pi, from which the

319 animals could partially recover (Fig 2D). Similarly, no radiological improvement was observed
320 between non-treated animals and animals treated with HCQ or HCQ in combination with
321 azithromycin, which was confirmed by quantification of micro-CT-derived biomarkers of lung
322 pathology (Fig 2E-G).

323 *Hydroxychloroquine and favipiravir fail to prevent SARS-CoV-2 infection in a transmission*
324 *model*

325 SARS-CoV-2 is typically transmitted through direct contact with respiratory droplets of an
326 infected person or from touching eyes, nose or mouth after touching virus-contaminated
327 surfaces. Transmission of SARS-CoV-2 through aerosols and direct contact has also been
328 demonstrated in a Syrian hamster model^{15,18}. We additionally explored whether SARS-CoV-2
329 can be transmitted via the fecal-oral route. To this end, hamsters that were intranasally
330 inoculated with virus were sacrificed at day 1 or day 3 pi. Subsequently, sentinel hamsters
331 were housed in the used cages of the index hamsters (food grids and water bottles were
332 replaced by fresh ones) and sacrificed at day 4 post exposure. Although viral RNA and
333 infectious virus could readily be detected in tissues from index hamsters (except in two stool
334 samples), the majority of sentinel hamsters did not become infected, as shown by the absence
335 of viral RNA and infectious virus in lung and ileum. (Supplemental Fig. 1). This indicates that
336 the fecal-oral route only marginally contributes to the transmission SARS-CoV-2 between
337 hamsters, thereby confirming the results of a previous study¹⁸. We therefore continued by
338 focusing on transmission of the virus via direct contact only.

339 Using the transmission model, we investigated the prophylactic potential of HCQ and favipiravir
340 against SARS-CoV-2. Sentinel hamsters received a daily dosage for 5 consecutive days with
341 either HCQ or favipiravir, starting 24 hours prior to exposure. Each individual sentinel hamster
342 was co-housed with an index hamster that had been intranasally inoculated with SARS-CoV-
343 2 the day before (Fig 3A). Index hamsters were sacrificed 4 days pi and sentinels 4 days post
344 exposure, after which the viral loads in lung, ileum and stool were determined. Index hamsters
345 had ~7 log₁₀ viral RNA copies/mg in the lungs, whereas untreated sentinel hamsters had

346 ~4 log₁₀ viral RNA copies/mg in the lungs (Fig 3B). Even though the variability between
347 individual hamsters in the sentinel groups was more pronounced than in the index groups, no
348 reduction in viral RNA was observed in either favipiravir- or HCQ-treated sentinel hamsters.
349 Also in ileum and stool, the viral RNA levels were not reduced by compound treatment. The
350 infectious viral loads in the lungs were also not reduced by treatment with either compound
351 (Fig 3C), which is in line with the viral RNA data. In contrast to index hamsters, sentinel
352 hamsters did not lose weight, but gained around 8% of body weight by day 4 pi. Sentinels that
353 received HCQ or favipiravir treatment gained less body weight than the untreated sentinels
354 (5% and 2%, respectively) (Fig. 3D). Pathology scores derived from micro-CT scans of
355 hamsters revealed multifocal pulmonary infiltrates and consolidations in some but not in all
356 hamsters (Fig. 3E, 3F). Also, micro-CT-derived biomarkers showed no difference in lung
357 pathology between untreated and treated sentinel hamsters (Fig. 3G), further confirming that
358 hydroxychloroquine and favipiravir failed to prevent SARS-CoV-2 infection in a transmission
359 model.

360 *Estimation of HCQ total lung and cytosolic lung concentrations*

361 Based on the measurement of trough concentrations of HCQ at sacrifice (n=14), a mean \pm SD
362 trough plasma concentration of 84 + 65 ng/mL (0.251 \pm 0.19 μ M) was found (Fig 4A). This is
363 comparable to the plasma trough concentrations that were detected in cynomolgus macaques
364 (treated with a dosing regimen of 90 mg/kg on day 1 pi (loading dose) followed by a daily
365 maintenance dose of 45 mg/kg)¹⁴ and in patients (3-5 days after starting treatment with 200
366 mg three times daily)¹⁴. The peak viral load in the lungs was not significantly associated with
367 plasma HCQ concentrations in individual hamsters (Fig 4B), suggesting that a higher HCQ
368 exposure did not result in a more pronounced reduction of viral infection.

369 According to Equation 1, a whole blood concentration of 1.804 \pm 1.39 μ M was calculated (Fig
370 4C). Subsequently, applying Equation 2, this resulted in a total lung concentration of 90.18 \pm
371 69.42 μ M, indicating that the lung tissues achieved HCQ concentrations above the reported *in*
372 *vitro* EC₅₀ values, ranging from 0.72 to 17.31 μ M, with a median value of 4.51 μ M and an

373 interquartile range of 5.44 (25-75%)²⁹. To estimate 90% of inhibition of viral replication (EC₉₀),
374 the EC₉₀ was equated to 3 times the EC₅₀, resulting in a target lung concentration of 13.53 ±
375 16.31 μM. In this case, the efficacy target at trough would be reached when applying this
376 dosing regimen (i.e., 50 mg HCQ sulphate/kg/day). However, it is important to note that the
377 total lung tissue concentrations described above consist of both intracellular and interstitial
378 HCQ concentrations. As the *in vivo* antiviral mechanism(s) of action of HCQ against SARS-
379 CoV-2 has not been clarified yet and might not be exclusively by inhibition of endosome
380 acidification³⁰, HCQ concentrations were calculated in cytosolic lung tissue, in the endosomal-
381 lysosomal compartment of cells and in the interstitial compartment. Assuming that cytosolic
382 HCQ concentrations are only 6% of total tissue concentrations, a total cytosolic lung tissue
383 concentration of 5.41 ± 4.17 μM was calculated. This value was in line with the median *in vitro*
384 EC₅₀ value, but is well below the estimated EC₉₀ value. Also the interstitial concentration was
385 calculated to be 5.41 μM. In contrast, the endosomal/lysosomal HCQ concentration was
386 calculated to be 1.9 mM, which is much higher than the estimated EC₉₀.

387 **Discussion**

388 In a previous study, we showed that wild-type Syrian hamsters are highly susceptible to SARS-
389 CoV-2 infections¹⁶. Here, we further characterized the hamster infection model to allow the use
390 of this model for antiviral drug evaluation. In agreement with previous studies, upon intranasal
391 inoculation, we observed that the virus replicates efficiently to peak levels (~6 log₁₀ TCID₅₀/mg)
392 in the lungs on day 4 pi., which is supported by radiological and pathological evidence.
393 Although the virus was also present in the ileum and stool of infected hamsters, levels were
394 significantly lower (~2.5 log₁₀ copies/mg). Besides serving as efficient replication reservoirs of
395 SARS-CoV-2, the hamsters also efficiently transmit the virus to co-housed sentinels^{15,18}. Here,
396 we demonstrated that the virus is mainly transmitted via direct contact and only to a limited
397 extent via the fecal-oral route. The variability observed in the virus titers in the lungs of the
398 sentinels is probably due to differences in the infection stage of the animals.

399 Besides hamsters, a variety of other animals have been tested for their permissiveness to
400 SARS-CoV-2, of which ferrets and non-human primates were the most sensitive ones³¹⁻³⁵. In
401 ferrets, infectious SARS-CoV-2 was only detected in the nasal turbinate and to a lesser extent
402 in the soft palate and tonsils, but not in the lungs³⁵. Although, in a different study infectious
403 virus in the lungs of ferrets was detected, levels remained close to the limit of detection³³. This
404 indicates that ferrets support SARS-CoV-2 replication, albeit to a lesser extent than hamsters.
405 In SARS-CoV-2-infected macaques (both rhesus and cynomolgus) virus levels were the
406 highest in nasal swabs and the lungs^{32,34}. SARS-CoV-2 infection resulted in moderate transient
407 disease in rhesus macaques, whereas cynomolgus macaques remained asymptomatic, but
408 did develop lung pathology as seen in COVID-19³⁴. Although aged macaque models may
409 represent the best models for studying more severe COVID-19 disease³⁶, both the high costs
410 and ethical considerations (leading to small group sizes) are major drawbacks of non-human
411 primate models. The efficient SARS-CoV-2 replication in the lungs of hamsters combined with
412 development of lung pathology endorses the use of hamsters over any other small animal
413 infection model for preclinical evaluation of the efficacy of antiviral drugs and immune-

414 modulating agents. Potent reduction of SARS-CoV-2 replication in hamsters has been
415 demonstrated by a single dose with a single-domain antibody from a llama immunized with
416 prefusion-stabilized coronavirus spikes^{16,37}, thereby validating the use of hamsters to evaluate
417 treatment options against SARS-CoV-2. In addition, our data also indicate that hamsters are
418 highly amenable for studying the potential antiviral effect of small molecules on virus
419 transmissibility in a pre- and post-exposure setting.

420 In an effort to contribute to the debate on the efficacy of (hydroxy)chloroquine and favipiravir
421 in COVID-19 patients, we evaluated both re-purposed drugs in our hamster infection and
422 transmission model. Treatment with HCQ or combined treatment with azithromycin was not
423 efficacious in significantly lowering viral RNA levels and infectious virus titers in the lungs of
424 SARS-CoV-2-infected hamsters. Lack of efficacy was also demonstrated in the transmission
425 model whereby sentinel hamsters were treated prophylactically prior to exposure to infected
426 hamsters. In SARS-CoV-2 infected ferrets, HCQ treatment was also not able to significantly
427 reduce *in vivo* virus titers³³. In addition, a recent study in SARS-CoV-2-infected cynomolgus
428 macaques showed that HCQ alone or in combination with azithromycin did not result in a
429 significant decrease in viral loads, both in a therapeutic and in a prophylactic setting¹⁴. On the
430 other hand, clinical trials with HCQ for the treatment of COVID-19 patients have resulted in
431 conflicting results and controversy. This is especially the case with clinical studies conducted
432 in the early stage of the pandemic, which were mostly small anecdotal studies. Results of large,
433 placebo-controlled, randomized trials are now becoming available. A randomized trial of HCQ
434 as post-exposure prophylaxis after high-to-moderate-risk exposure to COVID-19 showed that
435 high doses of HCQ did not prevent SARS-CoV-2 infection or disease similar to COVID-19³⁸.
436 In the RECOVERY trial, a large UK-based clinical study to evaluate potential therapies, HCQ
437 treatment did not result in a beneficial effect in mortality or hospital stay duration in patients
438 hospitalized with COVID-19³⁹. These data are in agreement with our results in the hamster
439 model and clearly underline the importance of preclinical studies in animal models in the drug
440 development/repurposing process.

441 The lack of effect observed for HCQ in this study and potentially also in other studies may be
442 explained by a pharmacokinetic failure. High lung concentrations of HCQ are caused by
443 massive accumulation ('ion trapping') of the compound in acidic lysosomes, which is driven by
444 a pH gradient between cytosol (pH 7.2) and lysosomes (pH 5). However, taking into account
445 the pH partition theory and considering the relative volumes of lung cellular and interstitial
446 compartments, only 6% of total HCQ concentrations in lung tissue is present in the cytosol of
447 lung cells. The other 94% of HCQ is present in the interstitial compartment and intracellularly
448 in lysosomes/endosomes or other subcellular fractions, or bound to proteins. Starting from the
449 measured trough concentrations from treated hamsters at day 4 or 5, the calculated HCQ
450 concentration in the endosomal compartment was 1.9 mM, which would be well above the
451 EC₉₀ target. In contrast, cytosolic concentrations in the lung were only slightly higher than the
452 EC₅₀ values reported in the literature, and far below the EC₉₀ target. Although alkalization of
453 endosomes has been proposed as one of the key mechanisms of the broad-spectrum antiviral
454 effect of HCQ, the mechanism of action against SARS-CoV-2 has not been completely
455 unraveled³⁰. Therefore, the very low cytosolic concentrations of HCQ in the lung may explain
456 the absence of an antiviral effect of HCQ against SARS-CoV-2 *in vivo*. Increasing the HCQ
457 dose to reach the EC₉₀ might not be feasible in terms of safety, as it may lead to an increased
458 risk of QTc prolongation and fatal arrhythmia. In future studies, lung tissue distribution of (re-
459 purposed) antiviral drugs should be taken into account, along with specification of the
460 subcellular target site, as recommended by Wang and Chen⁴⁰.

461 In contrast to HCQ, favipiravir was able to inhibit virus replication in intranasally infected
462 hamsters, but the effect was modest and only statistically significant at the viral RNA level. In
463 the transmission model on the other hand, favipiravir failed to reduce viral replication when
464 given as a prophylaxis. This suggests that the antiviral effect of favipiravir in COVID-19 patients
465 will most likely be limited. Also, the efficacy of favipiravir as a pre- or post-exposure prophylaxis
466 seems very modest. Clinical trials to evaluate the potency of favipiravir against SARS-CoV-2
467 are currently ongoing in China, Italy and the UK⁴¹. Prior, an open-label, randomized study

468 already showed that in COVID-19 patients with mild symptoms (fever and respiratory
469 symptoms without difficulties in breathing) the clinical recovery rate at day 7 was higher in the
470 favipiravir-treated group compared to the control group, which received treatment with
471 arbidol⁴². However, for COVID-19 patients with hypertension and/or diabetes as well as
472 critically ill patients, the clinical recovery rate was not significantly different between groups,
473 suggesting that favipiravir might be useful for patients with mild symptoms, but not for severely
474 ill patients. One concern with favipiravir is that it has been reported that the trough
475 concentrations (after 8-12h) in critically ill patients are lower than those in healthy persons and
476 do not even reach the *in vitro* obtained EC₅₀ value against SARS-CoV-2^{43,44}. This unfavorable
477 PK profile of favipiravir has been previously observed in Ebola virus-infected patients⁴⁵. While
478 favipiravir might be well tolerated and safe in a short-term treatment, safety concerns remain
479 as the drug proved to be teratogenic⁴⁶. Therefore, potential widespread use of favipiravir to
480 treat COVID-19 patients should be handled with caution.

481 In conclusion, we here characterize our hamster infection and transmission model to be a
482 robust model for studying the *in vivo* efficacy of antiviral compounds. Our data endorse the use
483 of Syrian hamsters as the preferred small animal model for preclinical evaluation of treatment
484 options against SARS-CoV-2. Our results also indicate that in both a therapeutic and a
485 prophylaxis scenario, a highly potent antiviral is necessary for a positive outcome. The
486 information we acquired using this model on HCQ and azithromycin is of critical value to those
487 designing (current and) future clinical trials. Of note, in a non-pandemic situation, based on the
488 pre-clinical data we provide, together with the earlier studies in ferrets and non-human
489 primates, there would be no indication to initiate clinical trials with either compound. We
490 recognize the exceptional situation the world is currently in and that clinical trials were initiated
491 at a time when no pre-clinical data was available. However, at this point, the pre-clinical data
492 obtained by us and others on HCQ and azithromycin provide no scientific basis for further
493 studies in humans with these molecules. The very modest reduction of viral load in the lungs
494 of hamsters treated with favipiravir and the lack of efficacy in the transmission model, also

495 suggests that the potential benefit of this drug in humans may be limited as well. Finally, we
496 emphasize the need to develop highly specific, potent and safe pan-corona antiviral drugs.
497 Highly potent drugs are available to treat other viral infections (such as with herpesviruses,
498 HIV, HBV, HCV and influenza virus) and it will without any doubt be possible, given sufficient
499 efforts, to develop also coronavirus inhibitors. Small animal infection models, such as the
500 hamster model, should have a pivotal place in (de)selecting drugs for clinical development.

501 **References**

502 1 Zhu N, Zhang D, Wang W, *et al.* A novel coronavirus from patients with pneumonia in
503 China, 2019. *N Engl J Med* 2020; **382**: 727–33.

504 2 Tay MZ, Poh CM, Rénia L, MacAry PA, Ng LFP. The trinity of COVID-19: immunity,
505 inflammation and intervention. *Nat Rev Immunol* 2020; 1–12.

506 3 Zhang B, Zhou X, Qiu Y, *et al.* Clinical characteristics of 82 death cases with COVID-
507 19. *medRxiv* 2020; 2020.02.26.20028191.

508 4 Delang L, Neyts J. Medical treatment options for COVID-19. *Eur Hear J Acute
509 Cardiovasc Care* 2020; published online May 4.

510 5 Jeon S, Ko M, Lee J, *et al.* Identification of antiviral drug candidates against SARS-
511 CoV-2 from FDA-approved drugs. *Antimicrob Agents Chemother* 2020.

512 6 Weston S, Haupt R, Logue J, Matthews K, Frieman M. FDA approved drugs with
513 broad anti-coronaviral activity inhibit SARS-CoV-2 in vitro. *bioRxiv* 2020;
514 2020.03.25.008482.

515 7 Keyaerts E, Vijgen L, Maes P, Neyts J, Ranst M Van. In vitro inhibition of severe acute
516 respiratory syndrome coronavirus by chloroquine. *Biochem Biophys Res Commun*
517 2004; **323**: 264–8.

518 8 De Wilde AH, Jochmans D, Posthuma CC, *et al.* Screening of an FDA-approved
519 compound library identifies four small-molecule inhibitors of Middle East respiratory
520 syndrome coronavirus replication in cell culture. *Antimicrob Agents Chemother* 2014;
521 **58**: 4875–84.

522 9 Delang L, Abdelnabi R, Neyts J. Favipiravir as a potential countermeasure against
523 neglected and emerging RNA viruses. *Antiviral Res* 2018; **153**.

524 10 Wang M, Cao R, Zhang L, *et al.* Remdesivir and chloroquine effectively inhibit the
525 recently emerged novel coronavirus (2019-nCoV) in vitro. *Cell Res* 2020; **30**: 269–71.

526 11 Choy KT, Wong AYL, Kaewpreedee P, *et al.* Remdesivir, lopinavir, emetine, and
527 homoharringtonine inhibit SARS-CoV-2 replication in vitro. *Antiviral Res* 2020; **178**:
528 104786.

529 12 Shannon A, Selisko B, Le T-T-N, *et al.* Favipiravir strikes the SARS-CoV-2 at its
530 Achilles heel, the RNA polymerase. *bioRxiv* 2020; 2020.05.15.098731.

531 13 Mehra MR, Desai SS, Ruschitzka F, Patel AN. Hydroxychloroquine or chloroquine with
532 or without a macrolide for treatment of COVID-19: a multinational registry analysis.
533 *Lancet* 2020.

534 14 Maisonnasse P, Guedj J, Contreras V, *et al.* Hydroxychloroquine in the treatment and
535 prophylaxis of SARS-CoV-2 infection in non-human primates. *Res Sq* 2020.

536 15 Chan JFW, Zhang AJ, Yuan S, *et al.* Simulation of the clinical and pathological
537 manifestations of Coronavirus Disease 2019 (COVID-19) in golden Syrian hamster
538 model: implications for disease pathogenesis and transmissibility. *Clin Infect Dis* 2020.

539 16 Boudewijns R, Thibaut HJ, Kaptein SJF, *et al.* STAT2 signaling as double-edged
540 sword restricting viral dissemination but driving severe pneumonia in SARS-CoV-2
541 infected hamsters. *bioRxiv* 2020. DOI:10.1101/2020.04.23.056838.

542 17 Spiteri G, Fielding J, Diercke M, *et al.* First cases of coronavirus disease 2019
543 (COVID-19) in the WHO European Region, 24 January to 21 February 2020.

544 18 *Eurosurveillance* 2020; **25**: 2000178.

545 18 Sia SF, Yan L-M, Chin AWH, *et al.* Pathogenesis and transmission of SARS-CoV-2 in
546 golden hamsters. *Nature* 2020.

547 19 Tett S, Cutler D, Day R, Brown K. A dose-ranging study of the pharmacokinetics of
548 hydroxy-chloroquine following intravenous administration to healthy volunteers. *Br J
549 Clin Pharmacol* 1988; **26**: 303–13.

550 20 Wei Y, Nygard GA, Ellertson SL, Khalil SKW. Stereoselective disposition of
551 hydroxychloroquine and its metabolites in rats. *Chirality* 1995; **7**: 598–604.

552 21 Yao X, Ye F, Zhang M, *et al.* In Vitro Antiviral Activity and Projection of Optimized
553 Dosing Design of Hydroxychloroquine for the Treatment of Severe Acute Respiratory
554 Syndrome Coronavirus 2 (SARS-CoV-2). *Clin Infect Dis* 2020; ciaa237.

555 22 Touret F, Gilles M, Barral K, *et al.* In vitro screening of a FDA approved chemical
556 library reveals potential inhibitors of SARS-CoV-2 replication. *bioRxiv* 2020;
557 2020.04.03.023846.

558 23 Liu J, Cao R, Xu M, *et al.* Hydroxychloroquine, a less toxic derivative of chloroquine, is
559 effective in inhibiting SARS-CoV-2 infection in vitro. *Cell Discov.* 2020; **6**: 1–4.

560 24 Reed LJ, Muench H. A simple method of estimating fifty per cent endpoints. *Am J
561 Epidemiol* 1938; **27**: 493–7.

562 25 Vandeghinst B, Goossens B, Van Holen R, *et al.* Iterative CT Reconstruction Using
563 Shearlet-Based Regularization. *IEEE Trans Nucl Sci* 2013; **60**: 3305–17.

564 26 Berghen N, Dekoster K, Marien E, *et al.* Radiosafe micro-computed tomography for
565 longitudinal evaluation of murine disease models. *Sci Rep* 2019; **9**: 1–10.

566 27 Velde G Vande, Poelmans J, De Langhe E, *et al.* Longitudinal micro-CT provides
567 biomarkers of lung disease that can be used to assess the effect of therapy in
568 preclinical mouse models, and reveal compensatory changes in lung volume. *DMM
569 Dis Model Mech* 2016; **9**: 91–8.

570 28 Poelmans J, Hillen A, Vanherp L, *et al.* Longitudinal, in vivo assessment of invasive
571 pulmonary aspergillosis in mice by computed tomography and magnetic resonance
572 imaging. *Lab Investig* 2016; **96**: 692–704.

573 29 Garcia-Cremades M, Solans BP, Hughes E, *et al.* Optimizing Hydroxychloroquine
574 Dosing for Patients With COVID-19: An Integrative Modeling Approach for Effective
575 Drug Repurposing. *Clin Pharmacol Ther* 2020; cpt.1856.

576 30 Quiros Roldan E, Biasiotto G, Magro P, Zanella I. The possible mechanisms of action
577 of 4-aminoquinolines (chloroquine/hydroxychloroquine) against Sars-CoV-2 infection
578 (COVID-19): A role for iron homeostasis? *Pharmacol Res* 2020; **158**.

579 31 Kim Y II, Kim SG, Kim SM, *et al.* Infection and Rapid Transmission of SARS-CoV-2 in
580 Ferrets. *Cell Host Microbe* 2020; **27**: 704-709.e2.

581 32 Munster VJ, Feldmann F, Williamson BN, *et al.* Respiratory disease in rhesus
582 macaques inoculated with SARS-CoV-2. *Nature* 2020; 1–7.

583 33 Park S-J, Yu K-M, Kim Y-I, *et al.* Antiviral Efficacies of FDA-Approved Drugs against
584 SARS-CoV-2 Infection in Ferrets. *MBio* 2020; **11**.

585 34 Rockx B, Kuiken T, Herfst S, *et al.* Comparative pathogenesis of COVID-19, MERS,
586 and SARS in a nonhuman primate model. *Science (80-)* 2020; **368**: eabb7314.

587 35 Shi J, Wen Z, Zhong G, *et al.* Susceptibility of ferrets, cats, dogs, and other
588 domesticated animals to SARS-coronavirus 2. *Science* (80-) 2020; **368**: 1016–20.

589 36 Cleary SJ, Pitchford SC, Amison RT, *et al.* Animal models of mechanisms of SARS-
590 CoV-2 infection and COVID-19 pathology. *Br J Pharmacol* 2020; : bph.15143.

591 37 Wrapp D, De Vlieger D, Corbett KS, *et al.* Structural Basis for Potent Neutralization of
592 Betacoronaviruses by Single-Domain Camelid Antibodies. *Cell* 2020; **181**.

593 38 Boulware DR, Pullen MF, Bangdiwala AS, *et al.* A Randomized Trial of
594 Hydroxychloroquine as Postexposure Prophylaxis for Covid-19. *N Engl J Med* 2020;
595 NEJMoa2016638.

596 39 Horby PW, Landray M. Press release: No clinical benefit from use of
597 hydroxychloroquine in hospitalised patients with COVID-19. 2020
598 <https://www.recoverytrial.net/files/hcq-recovery-statement-050620-final-002.pdf>
599 (accessed June 16, 2020).

600 40 Wang Y, Chen L. Lung tissue distribution of drugs as a key factor for COVID-19
601 treatment. *Br J Pharmacol* 2020; bph.15102.

602 41 Du Y, Chen X. Favipiravir: Pharmacokinetics and Concerns About Clinical Trials for
603 2019-nCoV Infection. *Clin Pharmacol Ther* 2020; cpt.1844.

604 42 Chen C, Huang J, Cheng Z, *et al.* Favipiravir versus Arbidol for COVID-19: A
605 Randomized Clinical Trial. *medRxiv* 2020; 2020.03.17.20037432.

606 43 Irie K, Nakagawa A, Fujita H, *et al.* Pharmacokinetics of Favipiravir in Critically Ill
607 Patients with COVID-19. *Clin Transl Sci* 2020; cts.12827.

608 44 Eloy P, Solas C, Touret F, *et al.* Dose rationale for favipiravir use in patients infected
609 with SARS-CoV-2. *Clin Pharmacol Ther* 2020; cpt.1877.

610 45 Nguyen THT, Guedj J, Anglaret X, *et al.* Favipiravir pharmacokinetics in Ebola-
611 Infected patients of the JIKI trial reveals concentrations lower than targeted. *PLoS*
612 *Negl Trop Dis* 2017; **11**: e0005389.

613 46 Pilkington V, Pepperrell T, Hill A. A review of the safety of favipiravir - a potential
614 treatment in the COVID-19 pandemic? *J virus Erad* 2020; **6**: 45–51.

615

616 **Acknowledgments**

617 We thank Kathleen Van den Eynde for excellent technical assistance. We thank Molecubes
618 and Bruker Belgium for their support with the implementation of the micro-CT installation, Jef
619 Arnout and Annelies Sterckx (KU Leuven Faculty of Medicine, Biomedical Sciences Group
620 Management) and Animalia and Biosafety Departments of KU Leuven for facilitating the
621 studies.

622 This project has received funding from the Covid-19-Fund KU Leuven/UZ Leuven and the
623 COVID-19 call of FWO (G0G4820N), the European Union's Horizon 2020 research and
624 innovation program under grant agreements No 101003627 (SCORE project), funding from
625 Bill and Melinda Gates Foundation under grant agreement INV-00636, the Stichting Antoine
626 Faes.

627 G.V.V. acknowledges grant support from KU Leuven Internal Funds (C24/17/061). C.C. was
628 supported by the FWO (FWO 1001719N). S.J. is supported by a PhD fellowship of the Fund
629 for Scientific Research Flanders (FWO). S.t.H. is supported by a KU Leuven internal project.
630 B.H. is a postdoctoral fellow of the Flemish Research Council (FWO - 12R2119N).

631 **Declaration of Interests**

632 The authors declare no competing interests.

633 **Figure legends**

634 **Figure 1. Kinetics of SARS-CoV-2 replication and lung disease in hamsters. (A)** Viral RNA
635 levels in the lungs, ileum and stool of infected Syrian hamsters. At the indicated time intervals
636 pi, viral RNA levels were quantified by RT-qPCR. **(B)** Infectious viral load in the lung expressed
637 as TCID₅₀ per mg of lung tissue obtained at day 4 pi. **(C)** Weight change as compared to the
638 weight at d0 in percentage at the indicated time intervals pi. **(A-C)** The data shown are medians
639 plus the individual hamsters represented as separate data points. **(D)** Representative
640 transversal lung μ CT-images on SARS-CoV-2 infected hamsters at baseline (0 d.p.i) and 3
641 d.p.i. Red arrows indicate infiltration by consolidation of lung parenchyma. **(E)** Representative
642 H&E images of lungs of SARS-CoV-2-infected hamsters at day 0 and day 4 pi. Red arrows
643 point at a lymphoid follicle. The blue arrowhead indicates apoptotic cells in the bronchial
644 epithelium.

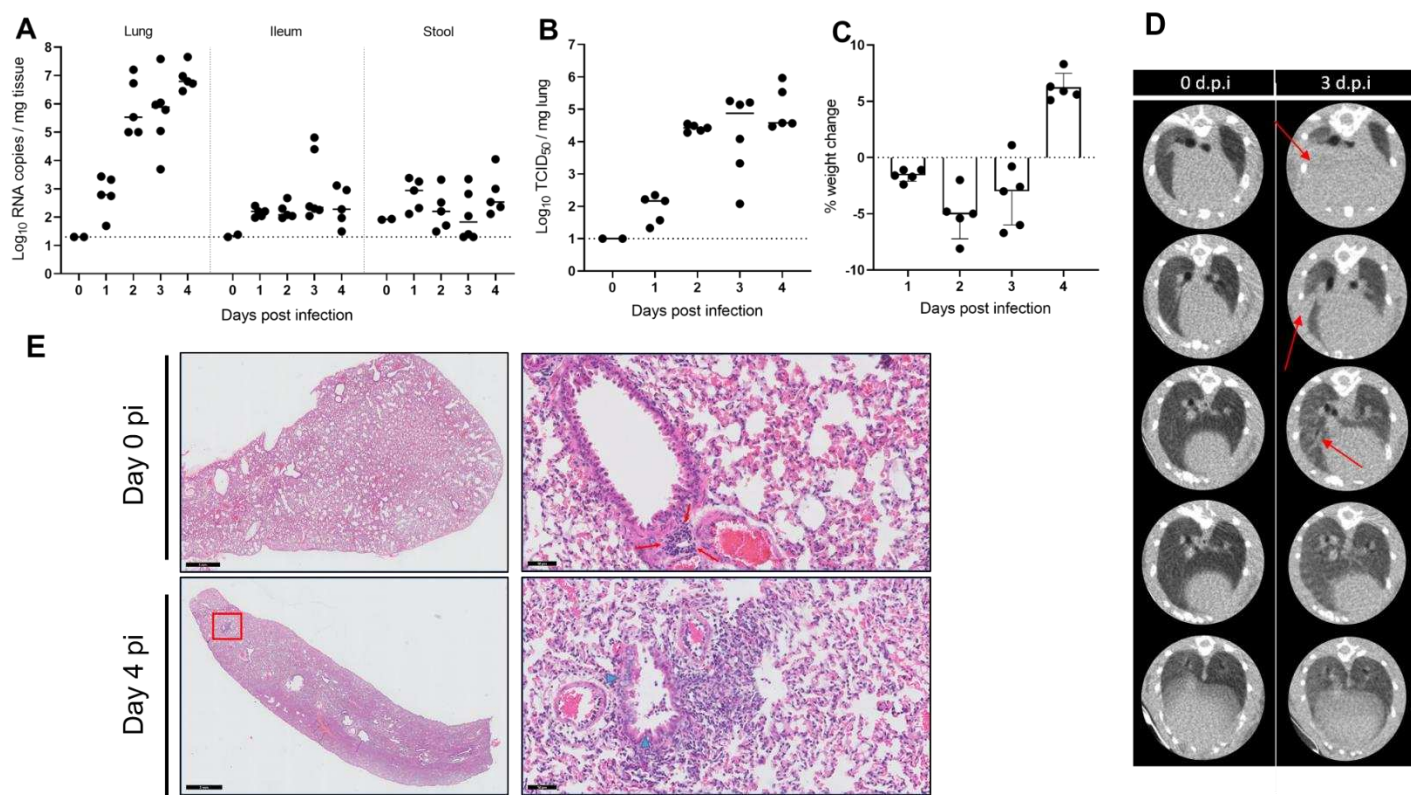
645 **Figure 2. *In vivo* testing of favipiravir and hydroxychloroquine (HCQ) in the SARS-CoV-
646 2 infection model. (A)** Set-up of the study. **(B)** Viral RNA levels in the lungs, ileum and stool
647 of untreated and treated (favipiravir, HCQ or HCQ + azithromycin) SARS-CoV-2 infected
648 hamsters at day 4 pi. At the indicated time intervals pi, viral RNA levels were quantified by RT-
649 qPCR. **(C)** Infectious viral load in the lung of untreated hamsters and hamsters receiving
650 treatment (favipiravir, HCQ or HCQ + azithromycin) expressed as TCID₅₀ per mg of lung tissue
651 obtained at day 4 pi. **(D)** Weight change of the hamsters as compared to the weight at d0 in
652 percentage points at the indicated time intervals pi. **(E)** Coronal lung μ CT images at 4 d.p.i. of
653 SARS-CoV-2 infected hamsters, untreated and treated with favipiravir, HCQ or HCQ +
654 azithromycin. Red arrows point to examples of pulmonary infiltrates observed as consolidation
655 of lung parenchyma. **(F, G)** Quantification of μ CT-derived biomarkers: non-aerated lung
656 volume (reflecting the tissue lesion volume) and aerated lung volume relative to total lung
657 volume **(F)** and mean density of the aerated lung volume **(G)**. **(H)** Cumulative severity score
658 from H&E staining of lungs of SARS-CoV-2 infected hamsters that were untreated (blue) or
659 treated with favipiravir (red), HCQ (green) or HCQ + azithromycin (green-yellow).

660 **Figure 3. HCQ and favipiravir fail to prevent infection in a direct contact transmission**
661 **model. (A)** Set-up of the study. **(B)** Viral RNA levels in the lungs, ileum and stool at day 4 pi
662 are expressed as \log_{10} RNA copies per mg tissue. Closed dots represent data from index
663 hamsters ($n = 5$) inoculated with SARS-CoV-2 one day before co-housing with sentinel
664 animals. Open dots represent data from sentinel hamsters ($n = 5$ per condition) which were
665 untreated (blue) or treated with either HCQ (green) or favipiravir (red), starting one day before
666 exposure to index animals. **(C)** Infectious viral loads in the lung at day 4 pi/post exposure are
667 expressed as \log_{10} TCID₅₀ per mg lung tissue. **(D)** Weight change at day 4 pi in percentage,
668 normalized to the body weight at the day of infection (index) or exposure (sentinel). **(E)**
669 Representative coronal and transversal lung μ CT images of sentinel favipiravir and
670 hydroxychloroquine (HCQ) treated hamsters at day 4 pi. Red arrows indicate examples of
671 pulmonary infiltrates seen as consolidation of lung parenchyma. **(F)** μ CT-derived biomarkers:
672 non-aerated lung volume (reflecting the tissue lesion volume) and aerated lung volume relative
673 to total lung volume of index SARS-CoV-2 infected hamsters and untreated, favipiravir and
674 HCQ treated sentinel hamsters. **(G)** Cumulative severity score from H&E staining of index
675 SARS-CoV-2 infected hamsters and untreated, favipiravir and HCQ treated sentinel hamsters.

676 **Figure 4. Pharmacokinetics of HCQ in infected and sentinel hamsters** **(A)** Individual
677 plasma trough concentrations of HCQ in hamsters treated with HCQ or HCQ and azithromycin
678 ($n=14$). **(B)** Viral RNA levels in lung tissue at day 4 pi to HCQ plasma trough concentrations of
679 individual hamsters. **(C)** Summary of trough blood and tissue levels of HCQ in hamsters dosed
680 with 50 mg/kg HCQ sulphate and comparison with *in vitro* EC₅₀ values.

681 **Figures**

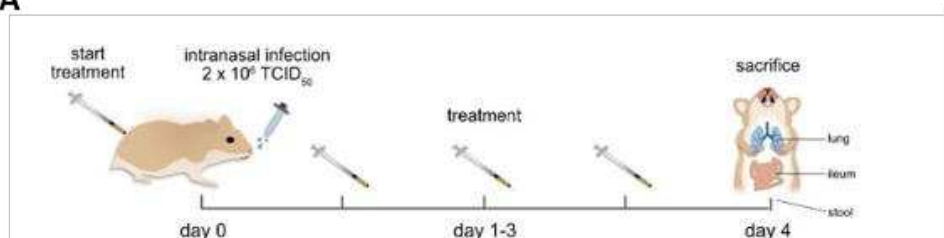
682 **Figure 1**



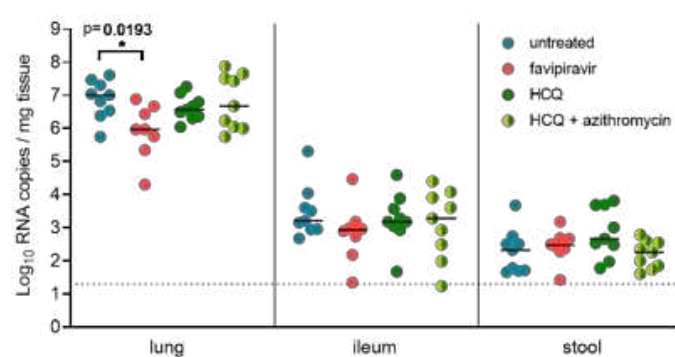
683

684 **Figure 2**

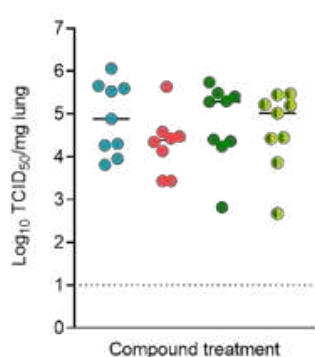
A



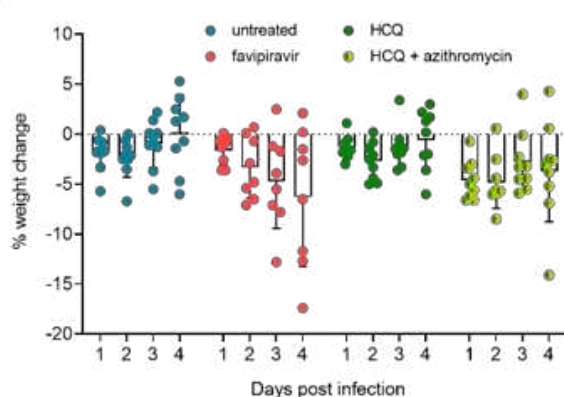
B



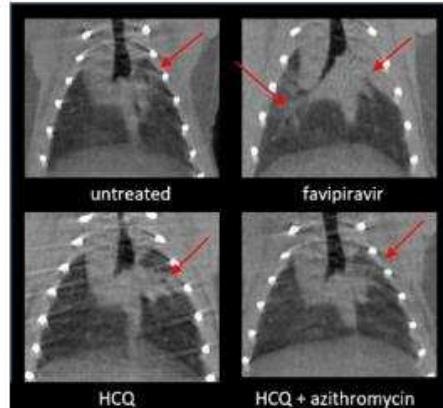
C



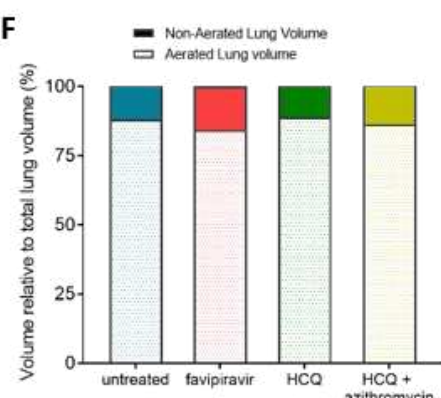
D



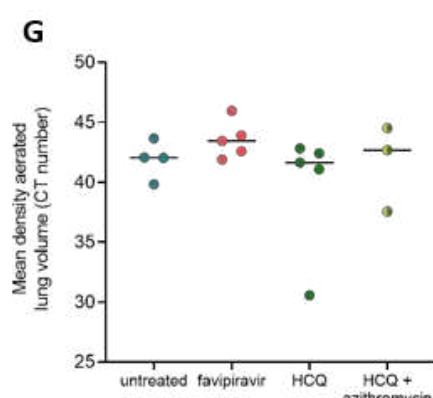
E



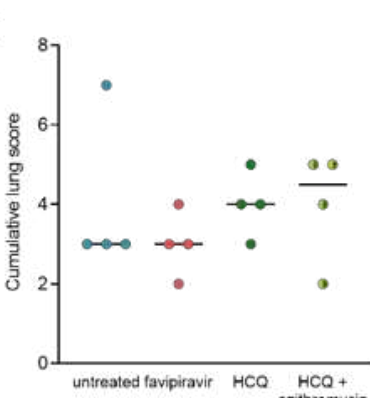
F



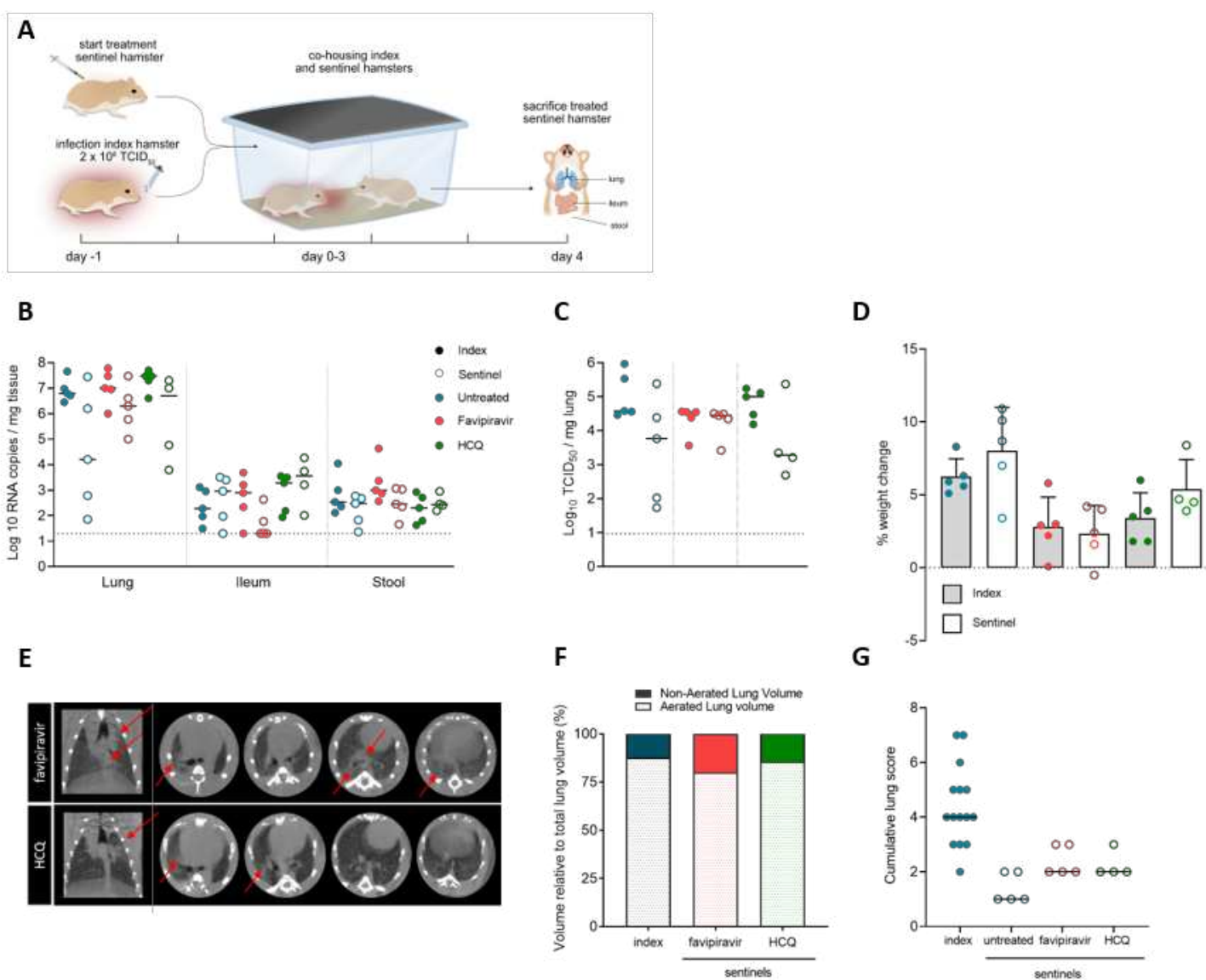
G



H

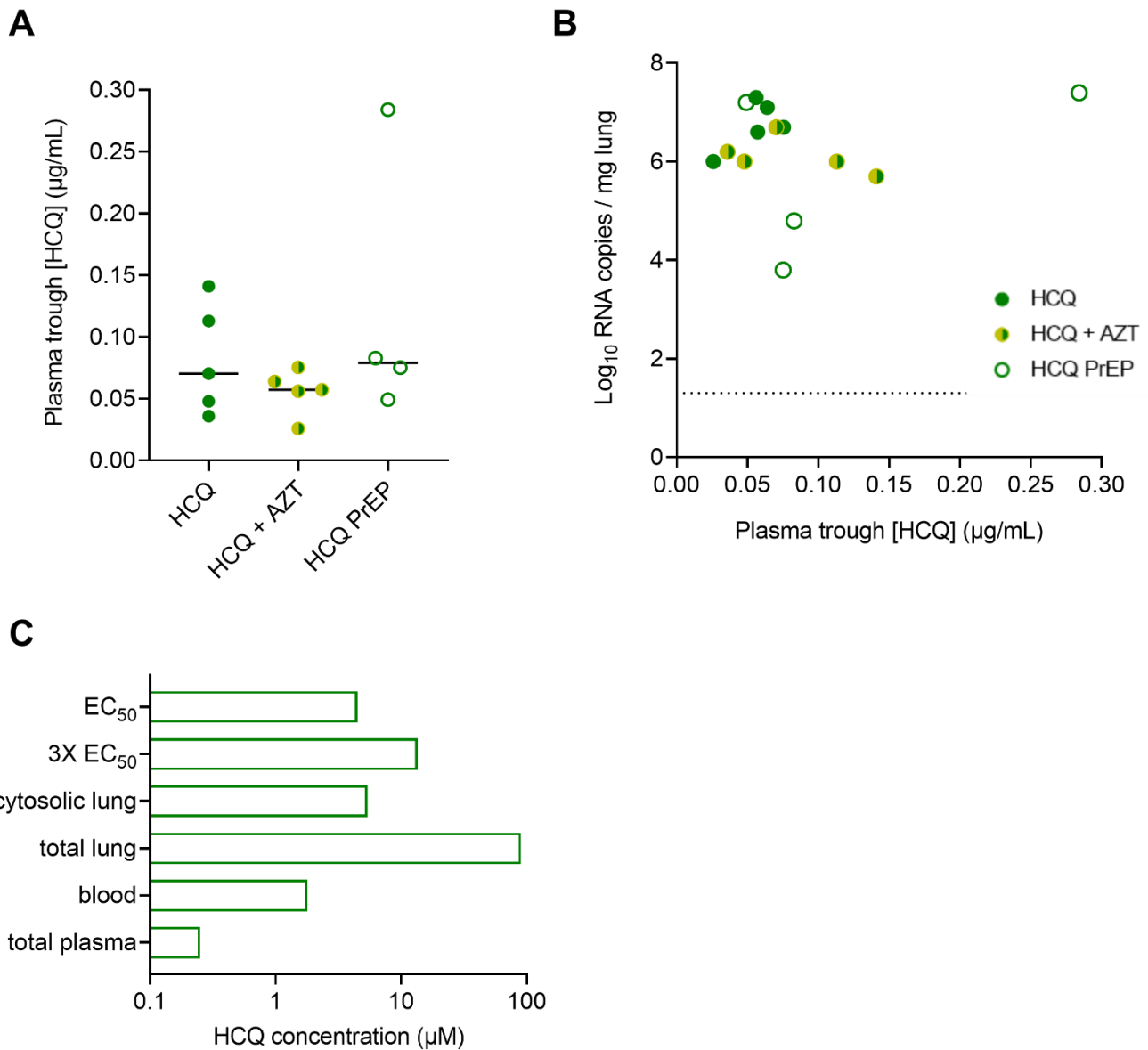


686 **Figure 3**



687

688 **Figure 4**



689